Supplementary Note 1: detailed description and diagnosis of the tessa model

October 16, 2020

1 Overview

T cells play a central role in moderating host immune response. T cell receptors (TCRs) identify specific TCR clonotypes and mediate recognition of antigens and activation of T cell. Therefore, an informative characterization of TCRs is critical for studying T cell immunity and responsiveness to immunotherapies. Many experimental and *in-silico* approaches have been developed to characterize the TCR repertoire. However, most existing approaches are not able to elucidate the functional relevance of TCR sequences, which significantly hinders and could mislead interpretation of the roles of T cells in various biological processes. To address this inadequacy, we developed a Bayesian model named tessa (**T**CR Functional Landscape **E**stimation **S**upervised with **S**cRNA-Seq **A**nalysis), to integrate TCR sequence profiling with the transcriptomes of T cells. Enabled by the recently developed single cell sequencing techniques, which provide both TCR sequences and RNA sequences of each T cell concurrently, tessa allows us to map the functional landscape of the TCR repertoire, and generates insights into understanding human immune response to diseases.

2 The tessa model

2.1 Input data

The aims of tessa include: (1) estimating TCR sequence similarities and building TCR networks, and (2) capturing the association between expression and TCR repertoire. The 10x Genomics Chromium single cell immune profiling technique, and other advanced sequencing techniques, are capable of providing both gene expression and T cell receptor sequencing for each T cell simultaneously. For each T cell, we have (1) gene expression levels, as one numerical vector. Each element in the vector represents the RNA expression level of one gene, and (2) one TCR sequence, which is converted into a numeric vector through a stacked auto-encoder. The TCR sequences considered in the tessa model include only the TCR-β chain CDR3 region sequences. Typically, one T cell has only one productive TCR-β chain detected. In very rare conditions when one T cell has two productive TCR-β chains detected from the sequencing data, we select the sequence with the higher expression level. The group of T cells from the same patient that share the same TCR sequence are referred to as the same clone, and they are of the same clonotype. No T cell appears in more than one clone, and there are some clones that have only one unique T cell. The stacked auto-encoder extracts sequence features from each unique TCR and converts it into a numerical vector. Let $i = 1, ..., T$ be the indices for T cells. Each T cell has a vector of numeric gene expression values, denoted by e_i, and a vector of numeric TCR sequence features, denoted by t_i.

2.2 Model specification

As the first step, T cells are assigned into networks depending on their sequence similarity, where T cells in one network are likely to target the same antigen. Naturally, T cells sharing the same TCR should be assigned to the same network. Therefore, networks are built on the units of TCRs, or clones, rather than those of T cells. We use t to represent all the unique TCRs, in the 30-dim embedded space, in one dataset. However, the RNA expression values of T cells sharing the same TCR are usually not the same, so we use e to represent expression of all individual T cells rather than T cell clones in one dataset. We consider identifying K networks among all T cells with observed data t and e. The number of networks K is a positive integer determined through a Dirichlet Process dynamically, which assigns the network membership $m_i \in \{1, ..., K\}$ for the $i-$th clone.

In each TCR network, we will determine a network center T cell clonotype. For the $k-$th network consisting of T cell clones with φ_k different TCR sequences $\{t_{k,1}, ..., t_{k,\varphi_k}\}$, we identify t_{k,c_k}, where $c_k \in \{1, ..., \varphi_k\}$, as the center TCR that is ”closest” to the mean of all embedded TCR sequences in this network. The remaining TCRs are considered as non-center in network k. Due to the inner structure of the networks such that there are center clones and non-center T cell clones in each network, we used the terminology of *networks* rather than *clusters* in this work, to emphasize this internal hierarchy.

Next, we maximize the association between TCRs and gene expression. Based on our observation of the real data, if two T cell clones within the same network have more similar TCRs, their expression profiles are also more similar. Motivated by this observation, we specify the relationship between TCR distances and expression distances in network k via a linear regression model,

$$d^e_{k,c_k,r} = a_k d^t_{k,c_k,r} + \epsilon_{k,r} \, , \tag{1}$$

where $d^t_{k,c_k,r}$ are distances between the center TCR and the non-center TCRs, $d^e_{k,c_k,r}$ represents the average of the pairwise distances, in terms of gene expression, between all T cells in the center clone and all T cells in each non-center clone, for $r = 1, ..., \varphi_k$. The regression coefficient and the random error are denoted by a_k and $\epsilon_{k,c_k,r}$, respectively. The error term $\epsilon_{k,c_k,r}$ is assumed to follow a normal distribution with mean 0 and a variance of σ^2_ϵ. Specifically, the two sets of distances in (1) can be calculated as,

$$d^t_{k,c_k,r} = \frac{1}{2}\sum_{q=1}^{Q} \frac{(t_{k,r,q} - t_{k,c_k,q})^2}{b_q}, 0 < r, c_k \in 1, ..., \varphi_k \, , \tag{2}$$

and,

$$d^e_{k,c_k,r} = \frac{\sum_{i\in g_{k,r}} \sum_{j\in g_{k,c_k}} ||e_i - e_j||^2}{|g_{k,r}| \cdot |g_{k,c_k}|}, 0 < r, c_k \in 1, ..., \varphi_k \, , \tag{3}$$

where $g_{k,r}$ and g_{k,c_k} refer to the sets of the cells that belong to non-center TCR clone $t_{k,r}$ and the center TCR clone t_{k,c_k}, respectively.

As we previously mentioned, the networks are built on TCR clones rather than T cells, and the transcriptomes of the T cells in the same clonotype are usually not the same. The expression distances in (3) are defined as the average of the expression distances between every cell in one clone and every cell in the other clone. Assuming that different embedding digits of TCRs have different importance in terms of describing the part of TCR that is more relevant for the function of T cells, we employ the weighting factor $b = \{b_q\}^Q_{q=1}$ in (2) to adjust the weights of each digit to maximize the association between expression and TCRs in (1). As a result, the component of TCRs that is more relevant to the function of T cells is more influential in the tessa model. Q is the number of embedding digits. For instance, $Q = 30$ with our stacked auto-encoder.

For the network assignments m_i ($m_i = 1, ..., K$) for clone i, we employ a Dirichlet Process with a very diffuse base measure, $G_0 : MVN((t_{mean,1}, ...t_{mean,i}, ..., t_{mean,30})^T, \lambda I_Q)$, where $t_{mean,i}$ represents the average value of the $i - th$ element of all the input embedded TCR sequences t, and λ is a large positive number which is pre-defined to keep the base measure diffuse enough and cover the dynamic region of the embedded TCR sequences. We define $t_{k,0}$ as the mean of the multivariate normal distribution that can describe the group of (embedded) TCRs in network k. We also define the center TCRs c_k, which is the TCR clonotype that is closest to $t_{k,0}$, and the fixed scaling parameter ξ for sampling m_i. We assume a multivariate normal distribution for t,

$$p(\{t_{k,1}, ..., t_{k,\varphi_k}\}|t_{k,0}, b, m_i) \propto \prod_{r=1,...,\varphi_k} \frac{e^{-d^t_{k,0,r}}}{(\prod b_q)^{0.5}} \, . \tag{4}$$

Given the network assignment in (4), for each network k, we define the center as,

$$c_k = \text{argmin}_s |t_{k,0} - t_{k,s}|, s \in \{1, ..., \varphi_k\} \, . \tag{5}$$

We then define priors and hyperpriors. A diffuse inverse gamma prior distribution $IG(u = 0.1, v = 0.1)$ is taken for b_q in (2) and for σ^2_e of the random error $\epsilon_{k,r}$ in (1). We assign the regression coefficient a_k in (1) with a $g-$prior $N(a, g\sigma^2)$. For the hyperparameter a, we assume a truncated normal prior to enforce a to have a positive value,

$$TN(a; 0, \tau, a > 0) \propto e^{-\frac{a^2}{2\tau}} \, , \tag{6}$$

where τ is a pre-defined large positive number to make the prior diffuse. The overall model structure is summarized in SN1 Fig 1.

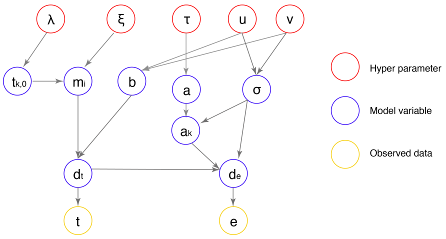

SN1 Fig. 1: The tessa model structure.

2.3 Posterior computation

Let $\Theta = \{\{a_k\}_{k=1}^{K}, \{b_q\}_{q=1}^{Q}, \{m_i\}_{i=1}^{K}, \{t_{k,0}\}_{k=1}^{K}, a, \sigma^2\}$ denote the set of model parameters. The joint posterior distribution is,

$$p(\Theta|t,e) \propto [\prod_{k=1}^{K} G_0(t_{k,0};\lambda)] \boldsymbol{.} [\prod_{q=1}^{Q} IG(b_q;u,v)] \boldsymbol{.} [\prod_{k=1}^{K} P(\{t_{k,1},...,t_{k,\varphi_k}\}|t_{k,0},\{b_q\}_{q=1}^{Q},m_i)] \boldsymbol{.} TN(a;0,\tau,a>0) \boldsymbol{.}$$
$$IG(\sigma^2;u,v) \boldsymbol{.} [\prod_{k=1,...,K} N(a_k|a,g\sigma^2)] \boldsymbol{.} [\prod_{k=1,...,K} \prod_{r=1,...,\varphi_k} N(d^e_{k,c_k,r}|a_k d^t_{k,c_k,r},\sigma_e^2)] \quad (7)$$

With the log-posterior in (8), we employ the MCMC sampling to draw samples for each parameter in Θ.

$$log(p(\Theta|t,e)) = -\sum_{k=1}^{K}\sum_{q=1}^{Q}\frac{t^2_{k,0,q}}{2\lambda} - \sum_{q=1}^{Q}[(u+1)log(b_q)+\frac{v}{b_q}] - \sum_{k=1}^{K}\sum_{r=1}^{\phi_k}[d^t_{k,0,r}+\frac{\sum_{q=1}^{Q}log(b_q)}{2}] - \frac{a^2}{2\tau} - [(u+1)log(\sigma^2)+\frac{v}{\sigma^2}]$$
$$-\sum_{k=1,...,K}[\frac{log(\sigma^2)}{2}+\frac{(a_k-a)^2}{2g\sigma^2}] - \sum_{k=1,...,K}\sum_{r=1,...,\varphi_k}[\frac{log(\sigma_e^2)}{2}+\frac{(d^e_{k,c_k,r}-a_k d^t_{k,c_k,r})^2}{2\sigma_e^2}]; a>0 \quad (8)$$

We update Θ according to the following steps.

(I) Updating network membership m_i for each cell i, using a Dirichlet process for all the clones $g_{k,r} = \{i|t_i = t_k, m_i = k\}$. The updating rule of each clone is as following,

(a) If this clone belongs to a network with $\varphi_k = 1$, we remove the network k, the associated $t_{k,0}$ and a_k, and update $\Lambda = \{1,...,K/k\}$.

(b) If this clone belongs to a network with $\varphi_k > 1$, we update the network k by changing φ_k to $\varphi_k - 1$.

Then we estimate the probability for each clone to belong to any of the existing networks or a new network following these steps.

(a) We build a new network $K+1$, the 'putative center' $t_{K+1,0}$ is drawn from $G_0(t_{K+1,0};\lambda)$ and the linear coefficient a_{K+1} is drawn from $N(a_{K+1}|a, g\sigma^2)$. The center of the new network is the clone $t_{k,r}$, which is denoted as $c_{K+1} = t_{k,r}$.

(b) We sample a network k_* from current networks, which includes the new one we created in the last step. The probability of drawing k_* from one of $\{\Lambda, K+1\}$ is proportional to

$$[I(k_* \in \Lambda)\varphi_k + I(k_* = K+1) \times 10^{\xi}] \boldsymbol{.} MN(t_{k,r}|t_{k_*,0},\{b_q\}_{q=1}^{Q}) \boldsymbol{.} N(d^e_{k_*,c_{k_*},r}|a_k d^t_{k_*,c_{k_*},r},\sigma_e^2)\,, \quad (9)$$

where $N(d^e_{k_*,c_{k_*},r}|a_k d^t_{k_*,c_{k_*},r},\sigma_e^2)$ refers to the regression between the TCR sequence and the T cell expression for the sampled k_*.

(c) We assign $t_{k,r}$ to the sampled k_* according to the last step. Update K if needed, and rename the associated indices including φ_k, m_i, $d^t_{k,c_k,r}$, $d^e_{k,c_k,r}$, and c_k.

(II) We update $t_{k,0,q}$ by drawing each $t_{k,0,q}$ from,

$$N(\frac{\sum_{r=1,...,\varphi_k} t_{k,r,q}}{b_q[\frac{1}{\lambda}+\frac{\varphi_k}{b_q}]}, [\frac{1}{\lambda}+\frac{\varphi_k}{b_q}]^{-1})\,. \quad (10)$$

(III) We update a_k by drawing each a_k from,

$$N(\frac{B_k}{A_k}, \sigma^2 A_k^{-1}), \tag{11}$$

where $A_k = \frac{1}{g} + \sum_{r=1,...,\varphi_k}(d^t_{k,c_k,r})^2$, and $B_k = \frac{a}{g} + \sum_{r=1,...,\varphi_k} d^e_{k,c_k,r} d^t_{k,c_k,r})$.

(IV) Then σ^2 is updated by $IG(C-1, D)$, where $C = u + 1 + \frac{K + \sum_{k=1,...,K}\varphi_k}{2}$, and $D = v + \frac{\sum_{k=1,...,K}[(a_k - a)^2 + g\sum_{r=1,...,\varphi_k}(d^e_{k,c_k,r} - a_k d^t_{k,c_k,r})^2]}{2g}$.

(V) Then a is updated by $TN(a; \frac{D}{E}, E^{-1}, a > 0)$, where $D = \frac{1}{\tau} + \frac{K}{g\sigma^2}$, and $E = \frac{\sum_{k=1,...,K} a_k}{g\sigma^2}$.

(VI) Next, we update all b_q for $q = 1, ..., Q$ at the same time. b_q is sampled by a Metropolis–Hastings (M-H) algorithm. The proposing function for each b_q is,

$$IG(u + \frac{\sum_{k=1}^{K}\varphi_k}{2}, v + \frac{\sum_{k=1}^{K}\sum_{r=1}^{\varphi_k}(t_{k,0,q} - t_{k,r,q})^2}{2}), \tag{12}$$

from where all $\{b_q^{'}\}_{q=1}^{Q}$ are sampled together, in order to calculate a new $(d^t_{k,c_k,r})^{'}$ in the next step. To decide the acceptance or the rejection of $\{b_q^{'}\}_{q=1}^{Q}$, the acceptance criterion is calculated as follows,

$$A(\{b_q^{'}\}_{q=1}^{Q}, \{b_q\}_{q=1}^{Q}) = min(1, e^{-F}), \tag{13}$$

where

$$F = \sum_{k=1,...,K}\sum_{r=1,...,\varphi_k}\frac{(d^e_{k,c_k,r} - a_k(d^t_{k,c_k,r})^{'})^2}{2\sigma_e^2} - \sum_{k=1,...,K}\sum_{r=1,...,\varphi_k}\frac{(d^e_{k,c_k,r} - a_k d^t_{k,c_k,r})^2}{2\sigma_e^2}. \tag{14}$$

2.4 Applying tessa to analyze T cells from multiple sources

Recent development of single-cell RNA-Seq technologies has allowed larger and larger library sizes in one experiment. It is common that tissue samples from different sources, for example, patients or mice, may be pooled and sequenced together. Such type of data can be analyzed together by tessa, which has the advantage of increasing sample size for parameter estimation and homogeneous inference across different subsets, *i.e.*, patients in the same datasets. In accordance, tessa implements the rule that TCR networks can only be built with T cells from the same subset of the data. Let us create an indicator function $I(g|g \in g_{k,r})$, which equals to 1 if the network $g_{k,r}$ contains only clones from the same source. Otherwise, if the network contains clones from more than one sources, we set $I(g|g \in g_{k,r})$=0. Then the joint posterior distribution in (7) is adjusted to,

$$\begin{aligned} p(\Theta|t,e) \propto [\prod_{k=1}^{K} G_0(t_{k,0};\lambda)] \cdot [\prod_{q=1}^{Q} IG(b_q;u,v)] \cdot [\prod_{k=1}^{K} P(\{t_{k,1},...,t_{k,\varphi_k}\}|t_{k,0},\{b_q\}_{q=1}^{Q},m_i)] \cdot TN(a;0,\tau,a>0) \cdot \\ IG(\sigma^2;u,v) \cdot [\prod_{k=1,...,K} N(a_k|a,g\sigma^2)] \cdot [\prod_{k=1,...,K}\prod_{r=1,...,\varphi_k} N(d^e_{k,c_k,r}|a_k d^t_{k,c_k,r},\sigma_e^2)] \cdot I(g) \end{aligned} \tag{15}$$

The additional requirement does not change any posterior sampling procedure, except for the sampling of network memberships. The DP probability needs to be updated as $p(k_*)I(g^{'})$, where $p(k_*)$ is the same as (9), and $I(g^{'})$ tests whether the potential assignment of k_* to $\{\Lambda, K+1\}$ is in compliance with the prerequisite that networks should only comprise clones from the same subset of data.

2.5 Linear relationship between TCR and expression of T cells

In this work, we assumed a linear relationship between TCR distances and expression distances of T cells in each network. One might argue that the linear relationship is not very obvious, as we showed in Extended Data. Fig. 2. In fact, in Extended Data. Fig. 2, these distances are calculated for all TCR clones of one dataset in a pair-wise manner. Therefore, in the right segments of each figure, where the TCR distances are large, such distances are more likely to be from pairs of T cells from different networks. In the left segments, the distances are more likely to be from pairs of T cells from the same networks. We only assume the intra-network distances to follow the linear relationship in the tessa model. As can be seen from Extended Data. Fig. 2, the relationship between TCR and expression in the left parts of the figures conform better to a linear relationship. For Extended Data. Fig. 2a, we subset the pairwise distances and kept only the top 10% pairs with the smallest TCR distances, likely more of which are intra-network pairs. The correlation coefficient increased from 0.493 (overall) to 0.784 (within this subset), as expected.

We also look further into the networks inferred by tessa and show that the intra-network pairs of the top three networks with the most TCR clones (SN1 Fig 2, dashed lines: regression line between expression distances and TCR distances, data from the healthy-CD8-3 dataset referred in the Supplementary Table.1). The intra-network expression and TCR distances confirm better to a linear relationship when viewed in this way.

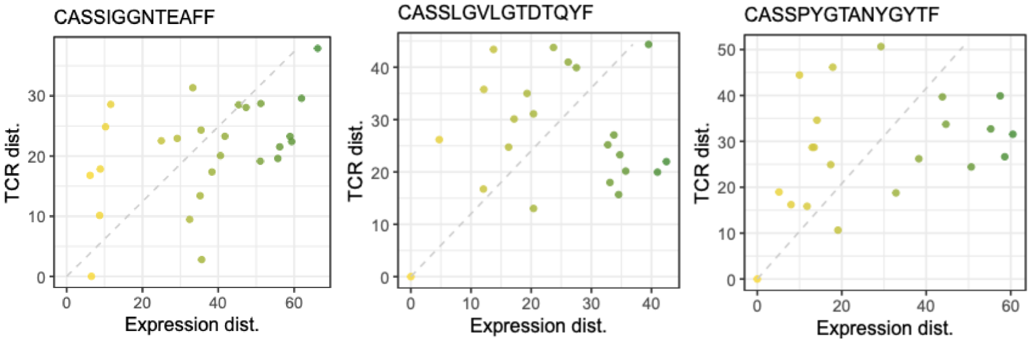

SN1 Fig. 2: Scatter plots showing the linear relationships between the intra-network distances.

On the other hand, assuming a linear model between TCRs and expression of T cells will have the advantage of being simple, which can avoid inadvertently forcing a very high and artificial correlation between TCRs and expression. But our future work can explore other possibilities of assuming non-linear relationships in the tessa model.

3 Simulation study

We conduct simulation studies to evaluate the performance of tessa under various settings. The simulation procedure is described as follows:

(a) We first define K networks for one simulation experiment denoted as $\Phi = \{\varphi_k\}$, for $k = 1, ..., K$, where φ_K, drawn from $U(1, 2\varphi_{ave})$, represents the number of clones of each network, and φ_{ave} is the average number of clones among K networks. Depending on K and Φ, we generate the simulated network memberships $M = \{m_i\}$, where $m_i \in 1, ..., K$, for each of the clone i. To simplify the simulation scheme, we skip the step of combining data from different T cells in the same clone when handling the real data. Instead, we directly generate the clone-level data.

(b) Each b_q, for $q \in 1, ..., Q$, is randomly drawn from an inverse-gamma distribution, the shape and the scale of which are determined to match the real data, we let $Q = 30$, the shape of the inverse-gamma distribution equals to 5, and the scale equals to 2.

(c) For each network, each element of the 'putative center' $t_{k,0}$ is randomly drawn from a normal distribution $N(0, (\frac{\sum_{q=1}^{Q} \sqrt{b_q}}{Q} \times t_{dist})^2)$, where $k \in 1, ..., K$, and t_{dist} is a diffusion factor that controls the overall TCR distances between network centers.

(d) For each network, the embedding of each TCR clonotype sequence is simulated from a normal distribution $N(t_{k,0,q}, b_q)$, where $q = \{1, ..., Q\}$, and φ_k different TCR sequences are simulated for the network k. All simulated TCR sequences are denoted as a matrix of t.

(e) Next, we calculate $d^t_{k,c_k,r}$ for all $k = 1, ...K$ with t and t_0. To simplify the calculation, here we assume that $t_{k,0}$ and c_k are the same, and both of them are real TCR centers for networks. Therefore, $d^t_{k,c_k,r} = \sum_{q=1}^{Q} \frac{(t_{k,r,q} - t_{k,0,q})^2}{b_q}$, where $k = 1, ...K$.

(f) Next we simulate the expression data for each network. We define a three-element expression vector for each clone. To simplify the simulation, we assume there are only three genes. Actually, any number of genes can be assumed, which has limited effect on the simulation results. Again, since the expression distance in tessa is calculated between two TCR clones, here we generate simulated expression data at the clonal level directly. For each network, each of the three elements of a 'putative expression center' $e_{k,0}$ is randomly drawn from a normal distribution $N(0, 100))$, where $k = 1, ..., K$, and we define the variance according to our observation of the real data. Only the center clones' expressions are simulated in this way. The other clones' expression are not simulated directly, but rather the clone-to-clone expressional distances are simulated as described below.

(g) Depending on the linear relationship we described in (1), for each of the network, $d^e_{k,c_k,r}$ is simulated from $d^t_{k,c_k,r}$. For each network k, the expression distance $d^e_{k,c_k,r}$ between clone r and center TCR c_k (which is replaced by $t_{k,0}$) is randomly drawn from $N(e_{k,0}, e^2_{dist} \times d^t_{k,c_k,r})$, where $k \in 1, ...K$, and e_{dist} is a diffusion factor that influences the approximate expression distances between network centers.

We consider the basic simulation setting with $K = 500$, $\varphi_{ave} = 10$, $t_{dist} = 1.5$, and $e_{dist} = 1$, to match the real data. Additioanl scenarios are considered in Section 3.3. For each scenario, we repeat the simulation study five times using different random seeds. The MCMC was iterated for 1,000 times, with the first 500 burn-ins.

3.1 Validation of the simulated data

To demonstrate that the data from our simulation experiments mimic real data, we first explored the simulated embedded TCRs with t-SNE plots (the same method as **Fig. 1e** in the main article) and one typical example (one simulated dataset with $K = 500$, $\varphi_{ave} = 10$, $t_{dist} = 1$, $e_{dist} = 1$) is shown in SN1 Fig 3. According to the simulation figure (SN1 Fig 3 below) and Fig. 1c of the main text, the ratios fo within and between network TCR distances, in the simulated and real data, are on a comparable scale.

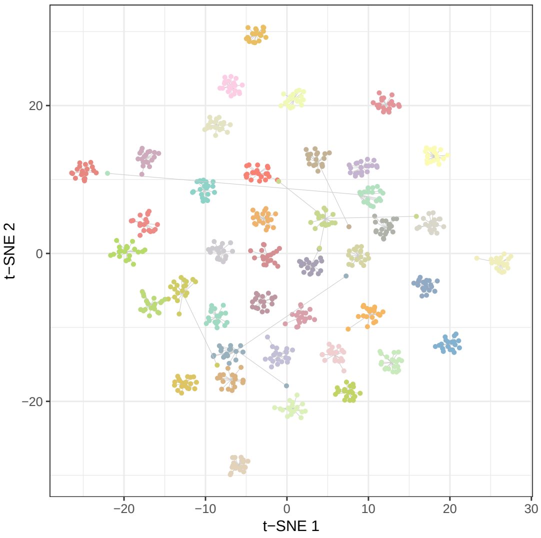

SN1 Fig. 3: T-SNE plots based on the TCR embeddings of the simulated TCR networks. TCRs in the same network were in the same color. Only the networks with more than 18 TCRs were shown to avoid the figures being overcrowded. The simulated TCR embeddings were adjusted by the simulated weighting factor b.

We further calculated the pair-wise TCR distances and expression distances of the simulated TCRs, and analyzed the correlation between the two sets of distances using the same method as in **Extended Data Fig. 2** in the main article. Typical examples (two simulated datasets with $K = 500$, $\varphi_{ave} = 10$, $t_{dist} = 1.5$, $e_{dist} = 1$, and different random seeds) were shown in SN1 Fig 4 (the r represents the Pearson correlation coefficient and the shaded area denotes the 95% confidence intervals for linear regressions). As expected, we found that the similar simulated TCRs were more likely to share similar simulated expression profiles, and the Pearson correlation coefficients between the two sets of distances were similar to those in the real datasets.

3.2 Diagnosis for convergence

We employed trace plots and auto-correlation functions (ACFs) to investigate the convergence of the MCMC process in the tessa model. Key parameters including a, and σ were examined. SN1 Fig 5a and SN1 Fig 6a shows that four parallel chains, initialized from four different random starting points, were well-mixed within 1000 iterations,

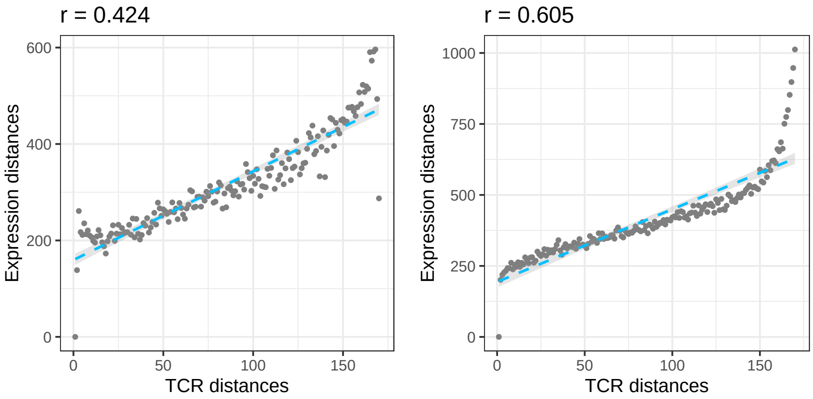

SN1 Fig. 4: Scatter plots showing the relationships between the distances of TCRs and the distances of RNA expression levels.

indicating convergence of of parameters a and σ in the tessa model. From SN1 Fig 5b and SN1 Fig 6b we found that the autocorrelations of the log-scaled parameters decreased to being not significantly different from zero at about lag 3, which indicates only small serial correlations and our trace plots are reliable diagnostics for convergence. Furthermore, we calculated the Gelman-Rubin statistic for all the key parameters, where b achieved a point estimate = 1.05 with 95% upper limit being 1.07. For a and σ, the point estimates were 1.07 and 1.11, and the 95% upper limit were 1.23 and 1.31, respectively. The Gelman-Rubin diagnostic results also suggested the MCMC procedure converged in tessa.

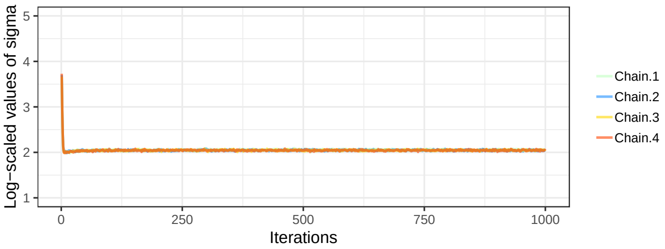

(a) Trace plots

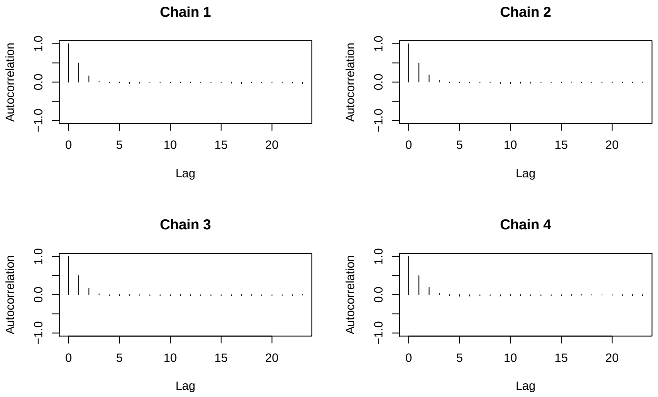

(b) Auto-correlation plots

SN1 Fig. 5: Trace plots and auto-correlation function plots of σ in four parallel chains.

3.3 Model performance evaluation

First we examined the 'accuracy' of the tessa networks measured by the Adjusted Rand Index (ARI). ARI estimates the similarity between the simulated clonal memberships $M_{sim} = \{m_1, m_2, ..., m_i, ..., m_N\}$, where $m_i \in \{1, 2, ..., K\}$ and N is the total number of clones, and the tessa predicted clonal meberships M_{pred}. An ARI of 0 represents random labeling, and 1 means that the M_{sim} and M_{pred} are identical. We vary the following parameters to create different

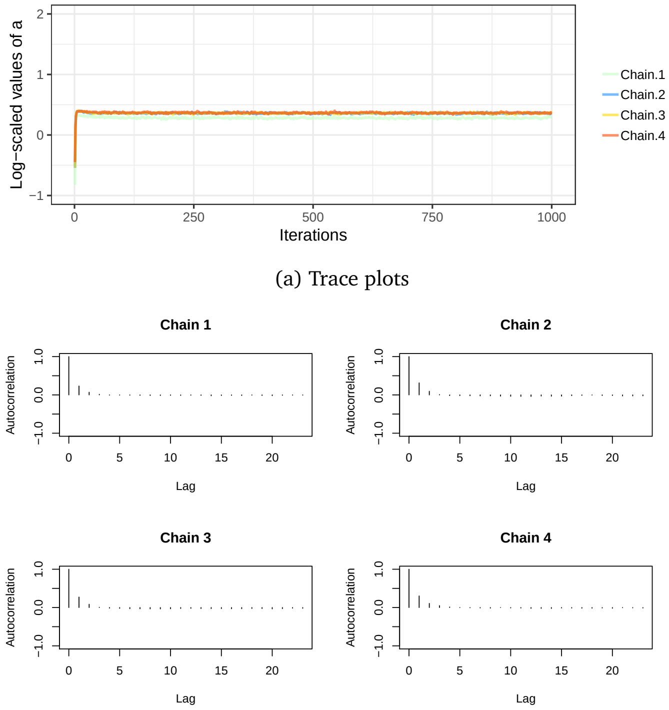

(a) Trace plots

(b) Auto-correlation plots

SN1 Fig. 6: Trace plots and auto-correlation function plots of a in four parallel chains.

simulation scenarios: $K \in \{100, 200, 300, ..., 900, 1000\}$, $\varphi_{ave} \in \{1, 2.5, 5, 7.5, 10, 12.5, 15\}$, $t_{dist} \in \{0.5, 1, 1.5, 2, 2.5, 3\}$, and $e_{dist} \in \{0.01, 0.1, 0.5, 1, 1.5, 2\}$. We varied one parameter at a time from the basic setting described in the end of simulation procedure. SN1 Fig 7a and SN1 Fig 7b showed that within the range of numbers used in the simulation, the number of the total TCR network in each dataset did not have much influence on the accuracy. However, building tessa networks with larger sizes achieved a higher modeling accuracy. We evaluated the real data and found that, mostly K is larger than 500 and smaller than 1000, and the average number of clones in the networks $\varphi_{ave} = 10$. Tessa has achieved high ARIs ($ARI > 0.90, SD < 0.10$) in the simulation tests within the range of the real data.

Next we evaluated whether the t_{dist}, the approximate TCR distances between networks, have influence on the accuracy. As we expected, increasing the t_{dist} resulted in a more dispersed network structure. Therefore, the results of tessa are more accurate as the networks become better separated by large distances (SN1 Fig 7c). In the real data, the estimated t_{dist} value is about 1.5. In SN1 Fig 7c we observed that tessa achieved $ARI = 0.94$ ($SD < 0.001$) when $t_{dist} = 1.5$. Next we evaluated the e_{dist}, which controls the clone-to-clone expression distances within networks. Increasing the e_{dist} resulted in higher ARIs, but the influence was limited (SN1 Fig 7d), which is expected as tessa does not primarily rely on the clones within the same network have similar or different expression profiles, but rather, emphasizes the regression between expression and TCRs within each network. In the real data, the estimated e_{dist} value ranges from 0.1 to 1. We found in SN1 Fig 7d that tessa achieved ARI between 0.91 and 0.94 ($SD < 0.001$) within the real data range of the e_{dist}.

Lastly, we evaluated the tessa estimations of the weighting factor b. As we elaborated in the main article, the weighting factor b weights the importance of each digit of the TCR sequence embedding, which respect to the expression of T cells. We compared the b_{sim} vectors that are simulated and the b_{pred} vectors from the tessa estmation results. Under all simulation conditions,the Pearson correlation coefficients were close to 1, with typical examples shown in SN1 Fig 8.

4 Hyper-parameter selection in real data

In the real data analysis, a standard diffuse prior was chosen for most hyper-parameters, and the inference is not sensitive to the choice of the value. There are two hyper-parameters that were tuned during the tessa model building, which are g and ξ. g is used in the prior for a_k in the formula (11). g stayed the same for all real datasets and had

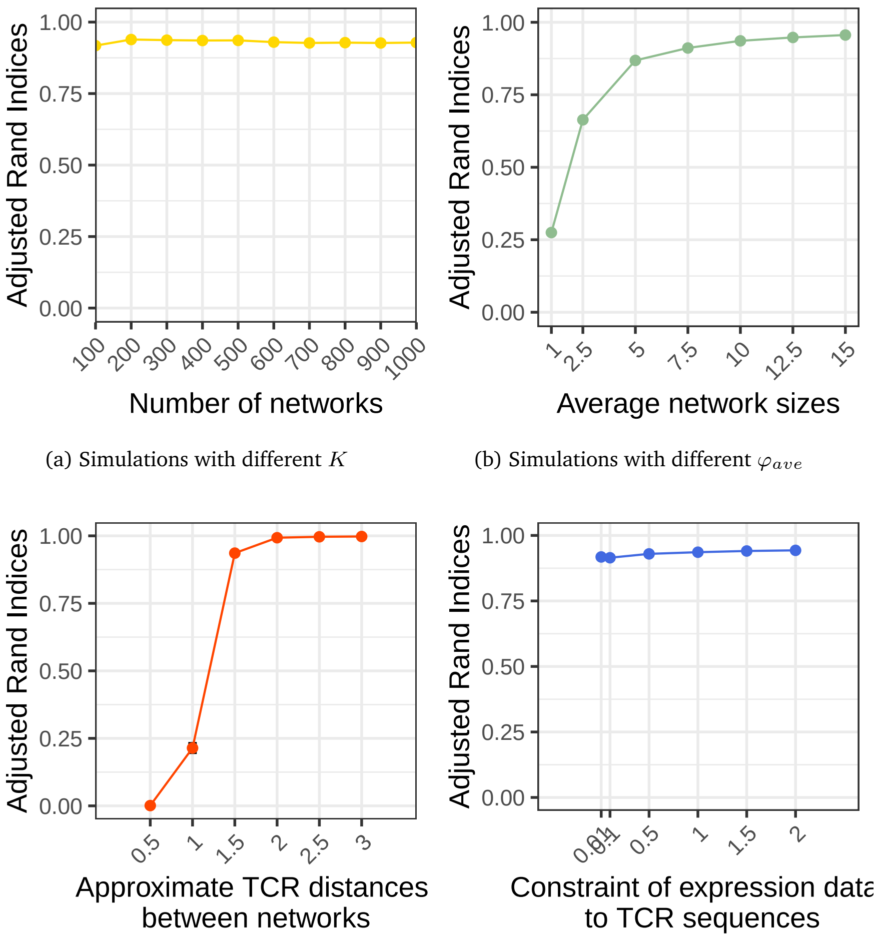

(a) Simulations with different K

(b) Simulations with different φ_{ave}

(c) Simulations with different t_{dist}

(d) Simulations with different e_{dist}

SN1 Fig. 7: ARIs of different simulation experiments. Error bars plotted as SDs of 5 random repeats, hard to be observed because of small differences.

limited effect on the final estimation outcome. g was chosen to be 0.001 to achieve the best convergence of the model. The hyper-parameter ξ is from the formula (9). ξ determines how likely TCRs are clustered into networks (larger number leads to fewer networks). ξ was 25 (default) for all datasets, except for the four healthy-CD8 datasets (Supplementary Table. 1), where ξ was 40. This choice was made to ensure the clustering rates of TCRs are comparable across the different datasets.

In summary, these simulation analyses have established the robustness of tessa, its good statistics characteristics, and its capability of accurately mapping the functional landscape of TCR repertoire.

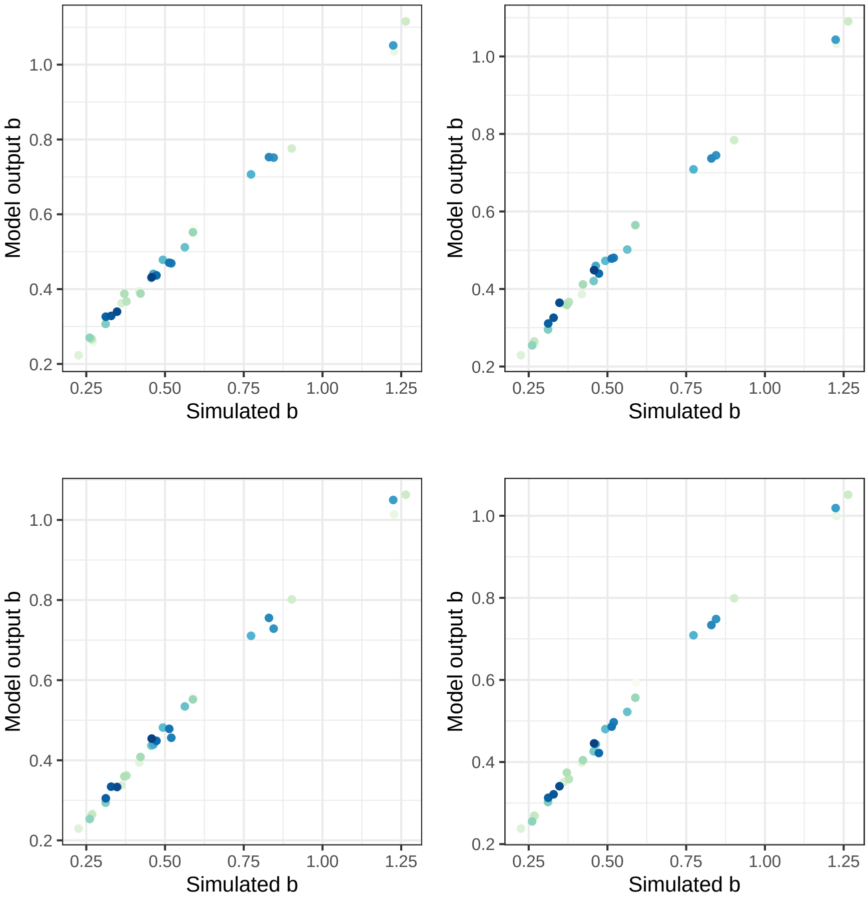

SN1 Fig. 8: Correlation between b_{sim} generated in the simulation and b_{pred} estimated by tessa.

Supplementary Note 2: Further bioinformatics analyses and discussion of tessa

Functional differences between center and non-center T cell clones

The 10X Immune Profiling technique (the 4 10X datasets) is very powerful and has incorporated multiple modalities. One of the modalities is the measurement of expression of a number of cell surface protein markers (in addition to regular scRNA expression). The captured markers for these cells include cell type sorting markers such as CD3 and CD8, and there are two, HLA-DR and PD-1, which can characterize T cell functional status. We examined the top 1% (in terms of network size) TCR networks that also have at least 3 different TCR clones, and divided the clones into three segments (group 1, group 2, and group 3), according to their tessa-weighted distances from the center clones, where group 1 are the most close clones to centers and group 3 are the most distant clones. We examined the expression of HLA-DR and PD-1 on T cells falling into each segment. It is quite interesting that, in each of the four datasets, a decreasing gradient can be seen, which means that T cells with TCRs more similar to the center TCRs have higher expression of HLA-DR and PD-1. As HLA-DR and PD-1 are markers of T cell activation[47-49], the results suggest that there is a gradient over group 1 to group 2 to group 3 such that the T cells with TCRs more similar to the center TCRs are more activated, consistent with their higher clonal expansion (**Fig. 2c-e**). For all boxplots appearing here and below, box boundaries represent interquartile ranges, whiskers extend to the most extreme data point which is no more than 1.5 times the interquartile range, and the line in the middle of the box represents the median.

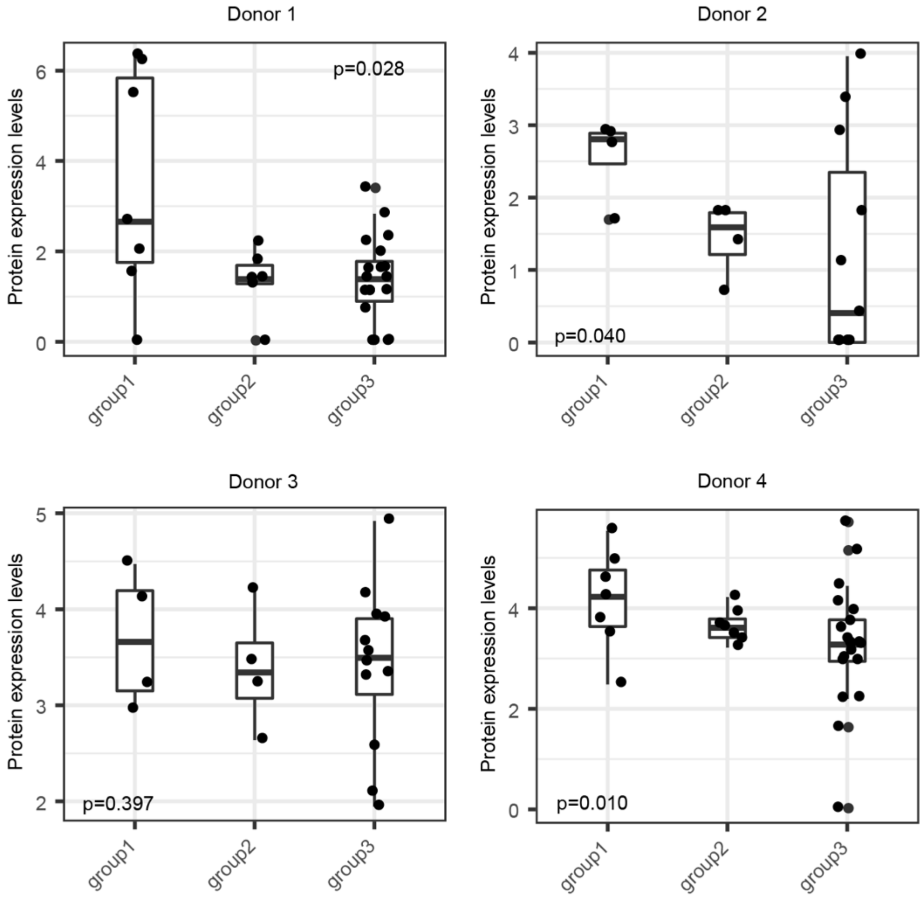

SN2 Fig. 1 *The expression of HLA-DR on the surface of the T cells in the TCR clones that were divided into group1, group2, and group3, across the 4 10X datasets. One-sided Jonckheere test was applied to test if there is a decreasing trend of HLR-DR expression from group 1 to group 3. The Fisher's combined p-value for the four datasets is 1.80x10-3. The number of clones in the three groups are: N1=7, N2=6, N3=19 (Donor 1), N1=4, N2=4, N3=11 (Donor 2), N1=4, N2=4, N3=12 (Donor 3), and N1=7, N2=7, N3=20 (Donor 4), respectively. Same for the figure below.*

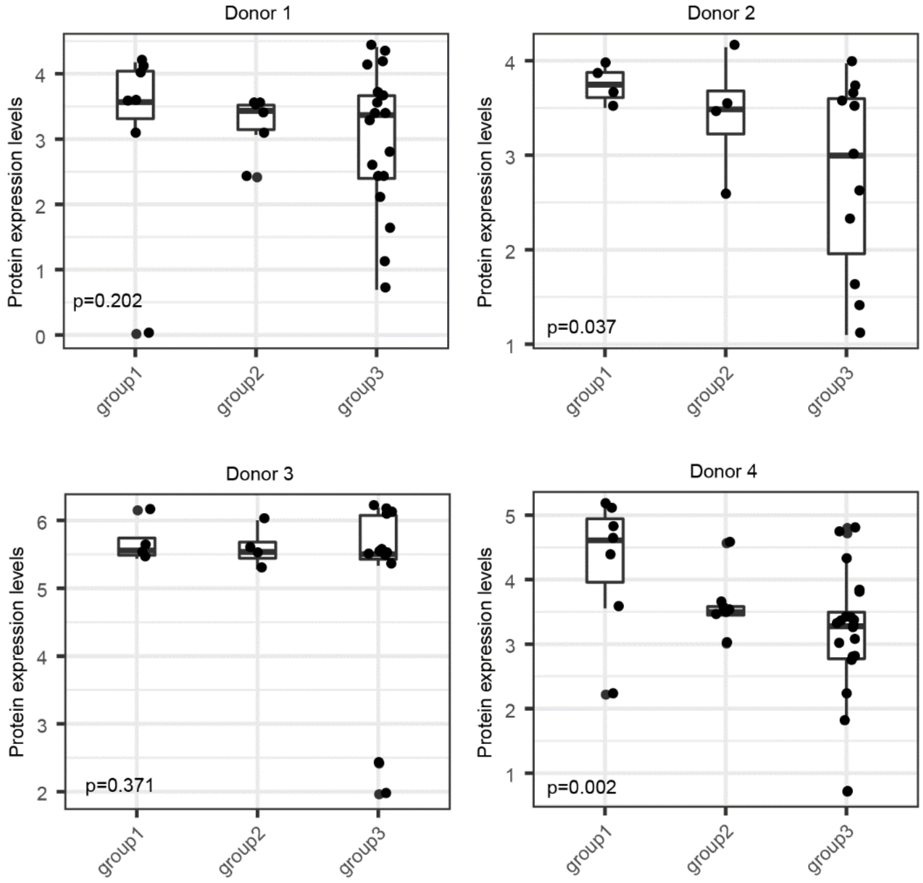

SN2 Fig. 2 *The expression of PD-1 on the surface of the T cells in the TCR clones that were divided into group1, group2, and group3, across the 4 10X datasets. One-sided Jonckheere test was applied to test if there is a decreasing trend of PD-1 expression from group 1 to group 3. The Fisher's combined p-value for the four datasets is 1.75*x*10^{-3}.*

Furthermore, using the RNA expression data of the T cells, we examined genes that showed a monotonous increasing or decreasing trend over group 1 to group 2 to group 3. We input them into the GOrilla server[50,51]. We found that, in these datasets, the monotonously changing genes are enriched in immune activation (group 1>group 2>group 3) and metabolomic terms (group 1<group 2<group 3), which echoes the PD-1 and HLA-DR results above. Due to the issue of space, we only show the Gene Ontology results from the first dataset. The P values shown are from two-sided Hypergeometric tests. The original P values and False Discovery Rates (FDRs) of multiple comparisons are both shown.

SF2 Table 1 *Up-regulated pathways in group 1 T cell clones*

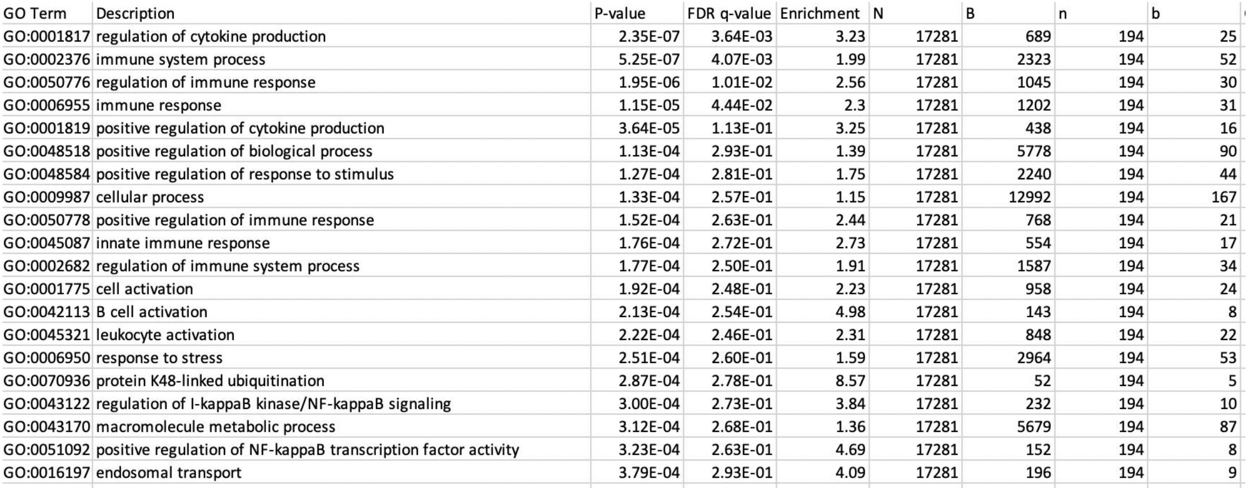

GO Term	Description	P-value	FDR q-value	Enrichment	N	B	n	b
GO:0001817	regulation of cytokine production	2.35E-07	3.64E-03	3.23	17281	689	194	25
GO:0002376	immune system process	5.25E-07	4.07E-03	1.99	17281	2323	194	52
GO:0050776	regulation of immune response	1.95E-06	1.01E-02	2.56	17281	1045	194	30
GO:0006955	immune response	1.15E-05	4.44E-02	2.3	17281	1202	194	31
GO:0001819	positive regulation of cytokine production	3.64E-05	1.13E-01	3.25	17281	438	194	16
GO:0048518	positive regulation of biological process	1.13E-04	2.93E-01	1.39	17281	5778	194	90
GO:0048584	positive regulation of response to stimulus	1.27E-04	2.81E-01	1.75	17281	2240	194	44
GO:0009987	cellular process	1.33E-04	2.57E-01	1.15	17281	12992	194	167
GO:0050778	positive regulation of immune response	1.52E-04	2.63E-01	2.44	17281	768	194	21
GO:0045087	innate immune response	1.76E-04	2.72E-01	2.73	17281	554	194	17
GO:0002682	regulation of immune system process	1.77E-04	2.50E-01	1.91	17281	1587	194	34
GO:0001775	cell activation	1.92E-04	2.48E-01	2.23	17281	958	194	24
GO:0042113	B cell activation	2.13E-04	2.54E-01	4.98	17281	143	194	8
GO:0045321	leukocyte activation	2.22E-04	2.46E-01	2.31	17281	848	194	22
GO:0006950	response to stress	2.51E-04	2.60E-01	1.59	17281	2964	194	53
GO:0070936	protein K48-linked ubiquitination	2.87E-04	2.78E-01	8.57	17281	52	194	5
GO:0043122	regulation of I-kappaB kinase/NF-kappaB signaling	3.00E-04	2.73E-01	3.84	17281	232	194	10
GO:0043170	macromolecule metabolic process	3.12E-04	2.68E-01	1.36	17281	5679	194	87
GO:0051092	positive regulation of NF-kappaB transcription factor activity	3.23E-04	2.63E-01	4.69	17281	152	194	8
GO:0016197	endosomal transport	3.79E-04	2.93E-01	4.09	17281	196	194	9

SF2 Table 2 *Up-regulated pathways in group 3 T cell clones*

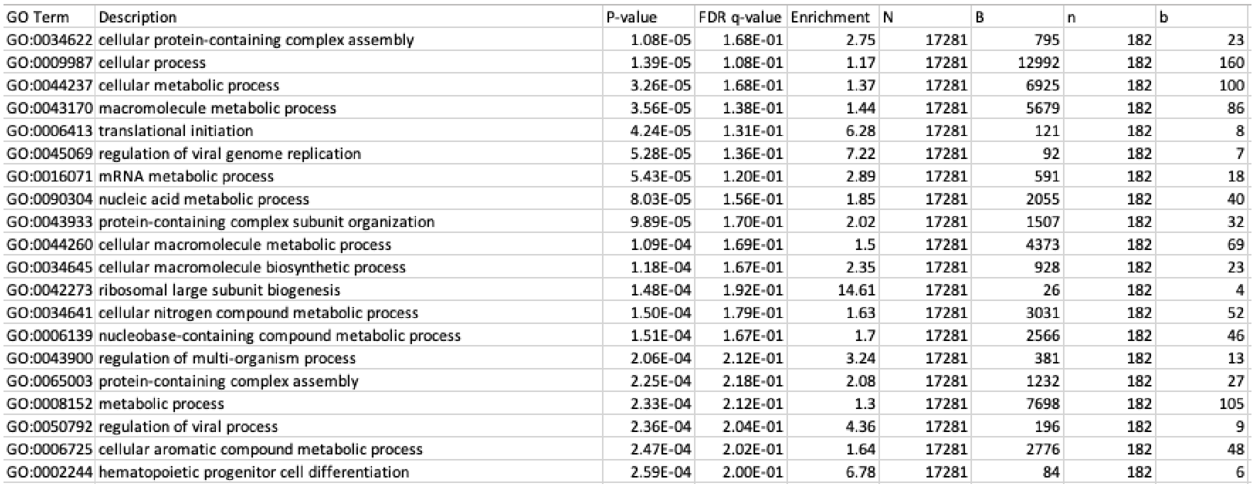

GO Term	Description	P-value	FDR q-value	Enrichment	N	B	n	b
GO:0034622	cellular protein-containing complex assembly	1.08E-05	1.68E-01	2.75	17281	795	182	23
GO:0009987	cellular process	1.39E-05	1.08E-01	1.17	17281	12992	182	160
GO:0044237	cellular metabolic process	3.26E-05	1.68E-01	1.37	17281	6925	182	100
GO:0043170	macromolecule metabolic process	3.56E-05	1.38E-01	1.44	17281	5679	182	86
GO:0006413	translational initiation	4.24E-05	1.31E-01	6.28	17281	121	182	8
GO:0045069	regulation of viral genome replication	5.28E-05	1.36E-01	7.22	17281	92	182	7
GO:0016071	mRNA metabolic process	5.43E-05	1.20E-01	2.89	17281	591	182	18
GO:0090304	nucleic acid metabolic process	8.03E-05	1.56E-01	1.85	17281	2055	182	40
GO:0043933	protein-containing complex subunit organization	9.89E-05	1.70E-01	2.02	17281	1507	182	32
GO:0044260	cellular macromolecule metabolic process	1.09E-04	1.69E-01	1.5	17281	4373	182	69
GO:0034645	cellular macromolecule biosynthetic process	1.18E-04	1.67E-01	2.35	17281	928	182	23
GO:0042273	ribosomal large subunit biogenesis	1.48E-04	1.92E-01	14.61	17281	26	182	4
GO:0034641	cellular nitrogen compound metabolic process	1.50E-04	1.79E-01	1.63	17281	3031	182	52
GO:0006139	nucleobase-containing compound metabolic process	1.51E-04	1.67E-01	1.7	17281	2566	182	46
GO:0043900	regulation of multi-organism process	2.06E-04	2.12E-01	3.24	17281	381	182	13
GO:0065003	protein-containing complex assembly	2.25E-04	2.18E-01	2.08	17281	1232	182	27
GO:0008152	metabolic process	2.33E-04	2.12E-01	1.3	17281	7698	182	105
GO:0050792	regulation of viral process	2.36E-04	2.04E-01	4.36	17281	196	182	9
GO:0006725	cellular aromatic compound metabolic process	2.47E-04	2.02E-01	1.64	17281	2776	182	48
GO:0002244	hematopoietic progenitor cell differentiation	2.59E-04	2.00E-01	6.78	17281	84	182	6

Further benchmarking tessa against GLIPH, for discovering novel biological insights

We carried out more systematic analyses to compare the results from tessa and also from GLIPH (purely TCR-based analyses) for the datasets used in **Fig. 234**, in order to demonstrate the capability of tessa in deriving novel biological insights in real data applications.

First we performed the analyses as we did in **Fig. 2e**, but with GLIPH. Here we show that GLIPH is not able to reveal the gradients of antigen binding affinity within the TCR clusters it identified.

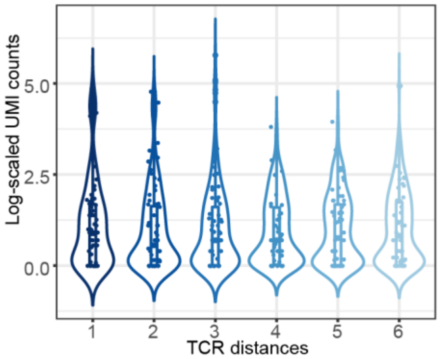

SN2 Fig. 3 *GLIPH cannot reveal the decreasing gradient of antigen binding strength for TCRs, along with increasing dissimilarity to the center TCRs of the TCR networks. The same analysis was done as in* ***Fig. 2e****, but with GLIPH instead of tessa. The TCR clonotypes from each dataset were divided into six groups of equal size (N(TCR)=198).*

We also performed GLIPH clustering on the BCC datasets of **Fig. 3**. As in our main text, we defined the 'pre-1, pre-2, post-1, post-2' subsets based on the clustering results. That is, post-2 clones are from clusters including only post-treatment clones, pre-2 clones are from pre-treatment-only clusters, and pre-1 and post-1 are from mixed clusters. We calculated pathway activity scores for the four subsets. The exhausted pathway is attached below. The figures show that GLIPH clustering is unable to distinguish post-treatment clones into two subsets, because all post clones were clustered with pre clones, leaving no post-treatment only clusters.

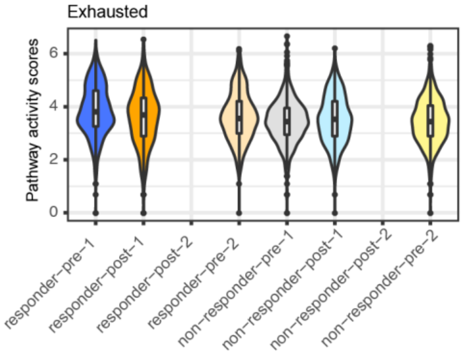

SN2 Fig. 4 *GLIPH clustering is unable to distinguish post-treatment cells into two subsets. The numbers of T cells in the six subgroups analyzed were: responders: N(pre-1)=1638, N(post-1)=830, N(pre-2)=859; non-responders: N(pre-1)=1023, N(post-1)=828, N(pre-2)=1029, respectively.*

Next we applied GLIPH clustering on all the single cell datasets and again calculated the 'unexplained variations' as we did in **Fig. 4d** to test the level of constraint on transcriptomic variations by TCRs, in the GLIPH clusters. In **Fig. 4d**, we took the top 20%, 40%, 60%, and 80% tessa networks with the largest numbers of unique TCR clones. But GLIPH identified much fewer clusters with each cluster being much bigger, in each dataset. Therefore, we cannot take this subsetting approach for GLIPH, and thus have showed all GLIPH clusters below:

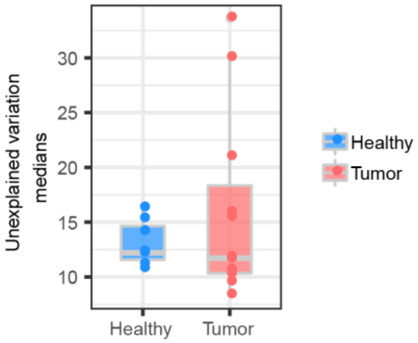

***SN2 Fig. 5** The unexplained variance in gene expression of all GLIPH clusters from twelve tumor samples of different cancer types and seven healthy donors.*

Our results show that, unlike tessa, GLIPH cannot reveal the differences in unexplained variations between tumor and normal scRNA datasets.

Controlling for T cell stages when interpreting the TCR-transcriptome associations

In **Fig. 4**, we derived the observation that the unexplained variations by TCRs are much larger for the tumor datasets than the normal datasets. As we discussed in our paper, TCRs and intrinsic/extrinsic cues both impact the functions of T cells, which is also the conclusions of Tubo *et al*[12] and Buchholz *et al*[13]. Therefore, it seems possible that the different levels of TCR/transcriptome association are strongly influenced by the differential stimulations in the tumor and normal contexts. To investigate this possibility, we divided the T cells into different stages, and refined our analyses in **Fig. 4d**.

We first categorized the T cells in each tumor/normal dataset into different functional states. As in Yost *et al*[31], we observed that the T cells formed a V-shaped distribution. At the joint of the two branches, are the naive cells and memory cells. The pseudotime analysis cannot distinguish the naive and memory cells, which is also the same as in Yost *et al*[31]. One of the branches has the activated cells and the other branch has the exhausted cells. We distinguished the activated and the memory cells by expression of marker genes. Specifically, we compared the average expression levels of five marker genes between the cells from the two branches. The cells in the activated branch should have higher expression levels of *IFNG*, *TNF* and *FOS*, and the cells in the exhausted branch should highly express *ENTPD1* and *HAVCR2*[31]. One example dataset was shown below (the Breast-1 dataset of **Supplementary Table 1**)

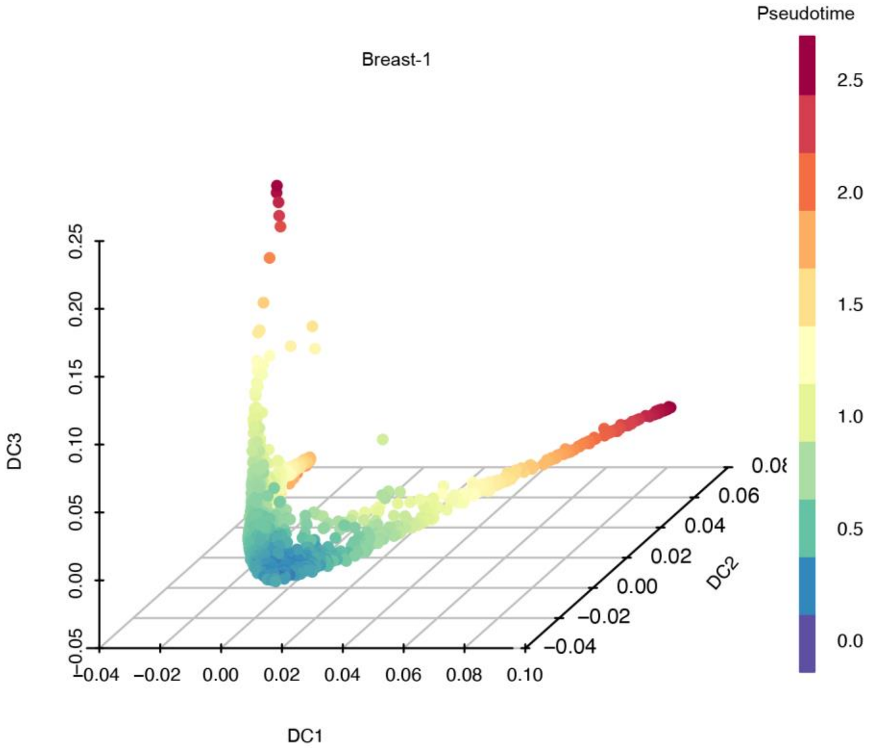

***SN2 Fig. 6** Pseudotime of T cells. The pseudotime of 2,403 T cells was inferred and overlaid onto the diffusion map.*

Next we repeated the analyses in **Fig. 4d** in each of the naive/memory, activated, and exhausted stages. In **Fig. 4d**, we carried out a percentage-wise sub-sampling approach at several cutoffs and observed the same phenomenon. Here, as we limited ourselves to a subset of T cells each time (*e.g.* naive/memory), this sub-sampling approach does not work, as we have lost sample sizes in this sub-sampling process. Therefore, the analyses below included all available cells.

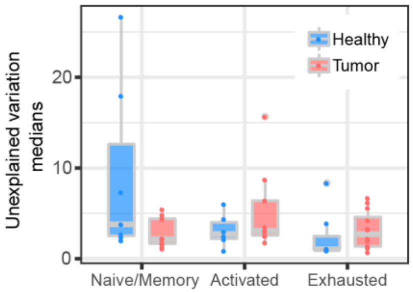

***SN2 Fig. 7** Unexplained variances by TCRs in each of the naive/memory, activated and exhausted stages in the twelve tumor datasets and seven healthy datasets.*

From the figure above, we make two interesting observations:

(1) The unexplained variances in the activated and exhausted cells in the tumor datasets are still larger than the normal datasets (P-values of 0.117 and 0.077 from one-sided Student's T-tests,

respectively), but the differences are smaller than in **Fig. 4d**. The unexplained variances in the naive/memory cells serve as a control (P-value of 0.186 from one-sided Student's T-test), which shows an opposite trend. These differences suggest that indeed the different functional statuses of T cells in tumor and normal contexts, as a consequence of differential stimulation, strongly influence how much TCRs constrain the functions of the T cells. Furthermore, the fact that activated and exhausted T cells still show more unexplained variances in tumor contexts than normal contexts suggest that there could be additional non-TCR-dependent cues from the tumor micro-environment that affected the functions of T cells that are supposed to be executing cytotoxic roles in tumor cells.

(2) On the other hand, in the normal contexts, T cells in the activated and exhausted stages have less unexplained variances by the TCRs than the naive/memory cells. But this phenomenon is reversed in the tumor context. This is also interesting, as in the normal contexts, the environmental cues are relatively quiescent, and TCRs may play more important roles in influencing T cell transcriptomics, when activated in a TCR-dependent manner. In comparison, the tumor microenvironment likely confers more complicated cues upon the T cells, especially the activated and exhausted subsets, so that TCRs of T cells could play less influential roles.

Re-coloring Fig. 3a

To make it easier to discern the different groups of patients (*e.g.* responder pre-1) in **Fig. 3a**, we have used 8 different colors to re-label these 8 different groups and shown the figure below.

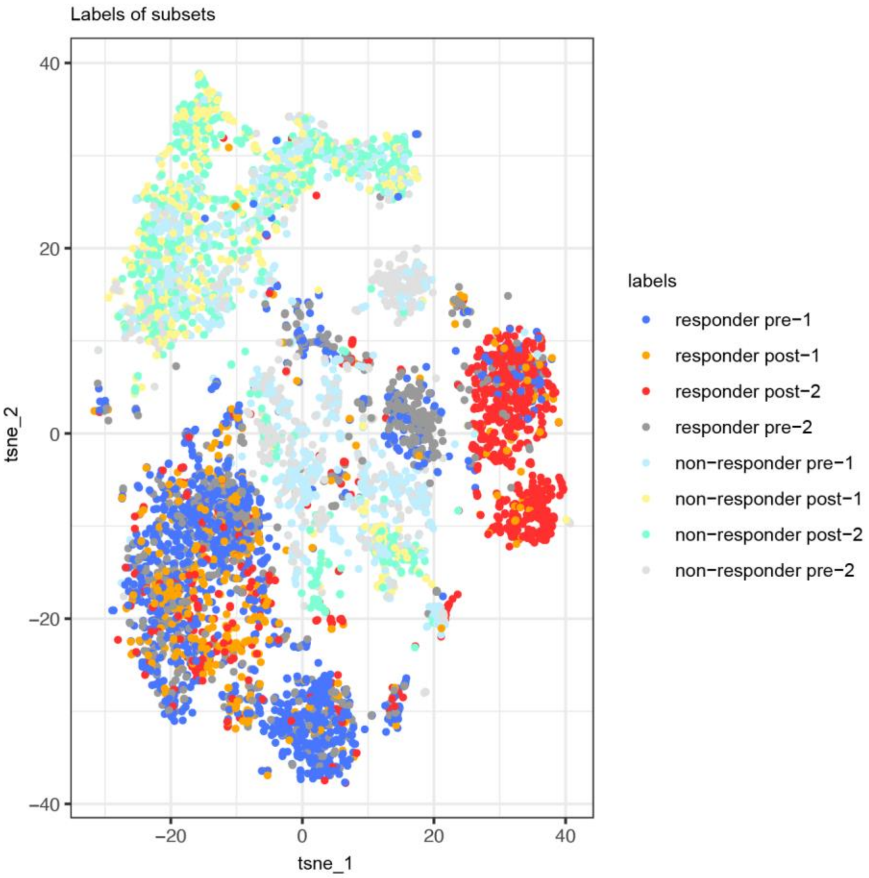

SN2 Fig. 8 *t-SNE plot of the pre- and post-treatment T cells from all the BCC patients (dataset BCC,* ***Supplementary Table 1****). The colors represent clonal level labels.*

This coloring scheme will make it easier to discern the 8 different groups of cells. But the coloring scheme in **Fig. 3a** makes it easier to be compared against **Fig. 3b**, which has a similar coloring scheme. We encourage the readers to consider these three figures together to visualize the changes between clone level labels and network level labels. The group of T cells that we want the readers to focus on is the “responder post-1” T cells, which is colored in orange in **SN2 Fig. 8**.

Quantifying the mixing effects of the clones in the CTCL patient and the healthy donor

For **Fig. 4ab**, we objectively quantified the mixing effects of the clones with Kullback-Leibler (KL) divergence between the original clonal distributions and randomly mixed distributions. For each dataset, we fixed the positions of cells on the t-SNE plot (**Fig. 4ab**) and gridded the t-SNE space into n x n (we selected n=10) squares. For cells from each clone, we calculated their frequency in the n^2 bins according to their t-SNE coordinates. Then we randomly permuted the clone labels of the cells and calculated their random frequency in these bins again. Then for each clone, a KL divergence statistic between the two sets of frequencies was calculated and regarded as ‘the relative difficulty for one clone becoming randomly distributed around the t-SNE space’.

The KL divergence calculation was repeated 1,000 times for each clone and the maximum S.D. across all the clones was 2.8. The 1,000 repeats were averaged to generate the KL divergence for each clone. As we show below, the healthy control clones have generally larger KL divergences. Therefore, the clone frequency distributions are less random or less 'mixed' than those from the CTCL patients. One-tailed student's t-test was performed between the two groups of KL divergence statistics, and the P-value was 0.011.

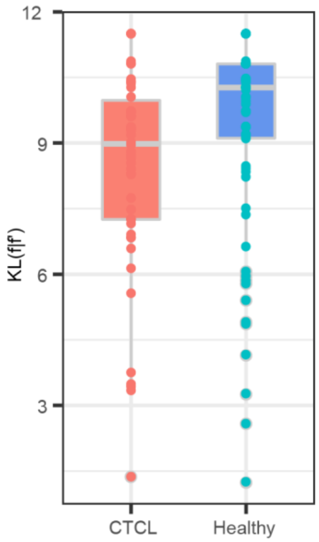

SN2 Fig. 9 *KL divergence statistics of the CTCL T cell clones and the healthy donor T cell clones for quantifying the mixing of the clones in the t-SNE space. N(CTCL)=416 and N(Healthy)=433.*

This KL divergence calculation used the true sample size and clone size information, which were the same for every round of simulation. Therefore, sample sizes and clone sizes were naturally controlled.

Additional discussion on the significance of tessa

Here we provide additional discussions of the significance of our work. They are adapted from the comments of one of our reviewers, whom we acknowledge deeply for providing such a nice summary of our work.

Tessa is built upon the landmark studies of GLIPH and TCRdist, which allowed for an analysis of 'likeness' or 'distance' between TCRs. Prior to this, TCRs were considered either clonally distinct or clonally identical, and therefore analyses of TCR repertoires were limited in that there was no provision for appreciating the 'effective diversity' of any epitope specific population. Our current study builds significantly on those by overlaying an analogous TCR distance algorithm with an analysis of transcriptional distance, which is of huge significance to the field especially in light of the numerous platforms now that support simultaneous resolution of both TCR sequences and transcriptional profiling. The bottleneck now really is in the analysis and interpretation of such parallel datasets and an algorithm, such as tessa, which aligns the two, would provide a substantial advance than what is currently available.

This work is powerful as it will provide not just critical fundamental information about the extent, to which TCR groupings are associated with distinct transcriptional profiles (and thus the extent to which the TCR is responsible for transcriptional phenotypes), but will enable the identification and selection of functionally potent TCR groupings when determined in the context of epitope specific populations. This in turn could facilitate the selection of TCRs for engineering/optimization/expression in clinical scenarios for the treatment of chronic viral infections or cancer immunotherapies. As an extension, one can imagine tessa facilitating the structural resolution of TCR recognition of pMHC class I proteins that drives a transcriptionally optimal phenotype. That is, by linking TCR clonotypes with transcriptional profiles, it will facilitate a deeper understanding of the key recognition characteristics that underpin this association.

References

47. Saraiva, D. P., Jacinto, A., Borralho, P., Braga, S. & Cabral, M. G. HLA-DR in Cytotoxic T Lymphocytes Predicts Breast Cancer Patients’ Response to Neoadjuvant Chemotherapy. Front. Immunol. 9, 2605 (2018).

48. Hong, J. J., Amancha, P. K., Rogers, K., Ansari, A. A. & Villinger, F. Re-evaluation of PD-1 expression by T cells as a marker for immune exhaustion during SIV infection. PLoS ONE 8, e60186 (2013).

49. Petrovas, C. et al. PD-1 is a regulator of virus-specific CD8+ T cell survival in HIV infection. J. Exp. Med. 203, 2281–2292 (2006).

50. Eden, E., Navon, R., Steinfeld, I., Lipson, D. & Yakhini, Z. GOrilla: a tool for discovery and visualization of enriched GO terms in ranked gene lists. BMC Bioinformatics 10, 48 (2009).

51. Eden, E., Lipson, D., Yogev, S. & Yakhini, Z. Discovering motifs in ranked lists of DNA sequences. PLoS Comput. Biol. 3, e39 (2007).

Supplementary Table 1 Data cohorts and details.

Cohort	Reference	Accession methods	#T cells	#Unique TRB sequences	Role	Data type
TCGA	Citation [23]	https://gdc.cancer.gov/about-data/publications/panimmune	204,881	181,787	Training auto-encoder	TCRs called from tumor RNA-Seq
Kidney-bulkRNA	Citation [24]	https://github.com/jcao89757/TESSA/tree/master/Tessa_released_data	80,801	75,157	Training auto-encoder	TCRs called from tumor RNA-Seq
IEDB	https://www.iedb.org/	https://www.iedb.org/database_export_v3.php	93	58	Training auto-encoder	TCR database export
McPAS	Citation [26]	http://friedmanlab.weizmann.ac.il/McPAS-TCR/	702	521	Training auto-encoder	TCR database export
NSCLC-1	Chromium Single Cell Immune Profiling Solution on the 10x website	https://support.10xgenomics.com/single-cell-vdj/datasets/2.2.0/vdj_v1_hs_nsclc_5gex	1,741	1,401	Training auto-encoder & Tessa	ScRNA-Seq multiplexed with TCR-Seq
NSCLC-2	Citation [26]	EGAS00001002430	3,628	845	Training auto-encoder & Tessa	ScRNA-Seq multiplexed with TCR-Seq
CRC	Citation [27]	EGAS00001002791	3,463	891	Training auto-encoder & Tessa	ScRNA-Seq multiplexed with TCR-Seq
HCC	Citation [28]	EGAS00001002072	3,536	2,506	Testing auto-encoder & Tessa	ScRNA-Seq multiplexed with TCR-Seq
Breast-1	Citation [29]	GSE114727, GSE114724	6,376	4,145	Training auto-encoder & Tessa	ScRNA-Seq multiplexed with TCR-Seq
Breast-2	Citation [29]	Same as above	6,289	4,028	Training auto-encoder & Tessa	ScRNA-Seq multiplexed with TCR-Seq
Breast-3	Citation [29]	Same as above	4,455	2,246	Training auto-encoder &	ScRNA-Seq multiplexed with TCR-

					Tessa	Seq
Breast-4	Citation [29]	Same as above	4,840	2,452	Training auto-encoder & Tessa	ScRNA-Seq multiplexed with TCR-Seq
Breast-5	Citation [29]	Same as above	4,189	2,243	Training auto-encoder & Tessa	ScRNA-Seq multiplexed with TCR-Seq
Healthy-CD8-1	Chromium Single Cell Immune Profiling Solution on the 10x website	https://www.10xgenomics.com/resources/application-notes/a-new-way-of-exploring-immunity-linking-highly-multiplexed-antigen-recognition-to-immune-repertoire-and-phenotype/	12,784	9,502	Tessa	ScRNA-Seq multiplexed with TCR-Seq
Healthy-CD8-2	Chromium Single Cell Immune Profiling Solution on the 10x website	Same as above	16,246	4,846	Tessa	ScRNA-Seq multiplexed with TCR-Seq
Healthy-CD8-3	Chromium Single Cell Immune Profiling Solution on the 10x website	Same as above	7,839	4,389	Tessa	ScRNA-Seq multiplexed with TCR-Seq
Healthy-CD8-4	Chromium Single Cell Immune Profiling Solution on the 10x website	Same as above	10,873	6,817	Tessa	ScRNA-Seq multiplexed with TCR-Seq
Healthy-PBMC-1	Chromium Single Cell Immune Profiling Solution on the 10x website	https://support.10xgenomics.com/single-cell-vdj/datasets/2.2.0/vdj_v1_hs_pbmc_5gex	709	589	Tessa	ScRNA-Seq multiplexed with TCR-Seq
Healthy-PBMC-2	Chromium Single Cell Immune Profiling Solution on the 10x website	https://support.10xgenomics.com/single-cell-vdj/datasets/3.0.0/vdj_v1_hs_pbmc2_5gex_protein	540	450	Tessa	ScRNA-Seq multiplexed with TCR-Seq
Melanoma	Citation [30]	GSE123139	3,615	1,690	Tessa	ScRNA-Seq multiplexed with TCR-Seq
BCC	Citation [31]	GSE113590	6,207	2,482	Tessa	ScRNA-Seq multiplexed with TCR-

						Seq
ECCITE-CTCL	Citation [16]	GSE126310	1,103	416	Tessa	ScRNA-Seq multiplexed with TCR-Seq
ECCITE-ctrl	Citation [16]	GSE126310	1,462	433	Tessa	ScRNA-Seq multiplexed with TCR-Seq
Glanville	Citation [10]	https://www.nature.com/articles/nature22976#MOESM1	704	207	Test antigen-specificity	TCR-antigen specificity data
Dash	Citation [11]	SRP101659	415	276	Test antigen-specificity	TCR-antigen specificity data

Supplementary Table 2 The genes in the T cell functional pathways related to **Fig. 3e-g** and **Extended Data Fig. 6.**

Naive	Memory	Activated	Exhausted	Inhibition
IL7R	*GZMK*	*IFNG*	*GZMB*	*TGFB1*
PABPC1	*CST7*	*JUNB*	*GNLY*	*LDHA*
CCR7	*DUSP2*	*SLC2A3*	*ENTPD1*	*FTH1*
RPS12	*SH2D1A*	*CD69*	*PRF1*	*SRGN*
FTH1	*TRAT1*	*NFKBIA*	*KRT86*	*MTRNR2L8*
LTB	*TC2N*	*PPP1R15A*	*ACP5*	*SRSF2*
ANXA1	*CMC1*	*TNF*	*GZMH*	*CREM*
TCF7	*LITAF*	*NR4A2*	*GAPDH*	*RPS26*
S1PR1	*EOMES*	*FOS*	*AC092580.4*	*SH2D2A*
RPL13	*GIMAP4*	*CCL4*	*GALNT2*	*PABPC1*
MT-ND2	*CNN2*	*NR4A1*	*ITGAE*	*HNRNPUL1*
EEF1B2	*COTL1*	*DUSP1*	*LAYN*	*ATP1B3*
CD55	*RPS15A*	*HSPA1B*	*CTSW*	*ZFP36*
	CXCR3	*IER2*	*CXCL13*	
	LDHA	*GADD45B*	*TNFRSF18*	
	RPS26	*JUN*	*AHI1*	
	TRMO	*CSRNP1*	*CXCR6*	
	FAM102A	*CDKN1A*	*VCAM1*	
	APOBEC3G	*TSC22D3*	*JAML*	
	MTRNR2L8		*ALOX5AP*	
	IL9R		*LAG3*	
	TGFB1		*LSP1*	
	HLA-B		*PTMS*	
	PLP2		*HLA-DRB1*	
	CCR7		*HLA-DPB1*	
			CCL5	
			CD74	
			HLA-DRA	
			HLA-DPA1	

Supplementary Table 2 The genes in the T cell functional pathways related to **Fig. 4e**.

IL-2 pathway #1	IL-2 pathway #2	IFN-a/b	IL-12 pathway #1	IL-12 pathway #2	Control pathway #1
IRF4	*NUP62*	*APBA2*	*DCAF17*	*TPTE*	*IPMK*
CD69	*ESM1*	*ZNF574*	*PAPPA2*	*CUL2*	*INPP5D*
BATF	*NPLOC4*	*ZNHIT3*	*C2orf88*	*CCDC70*	*ALAS2*
CCR7	*TMPO*	*ZDHHC9*	*AVEN*	*FANCM*	*YWHAE*
IL2RA	*CD81*	*XCR1*	*MB21D1*	*CEP192*	*ATG4B*
PRDM1	*APIP*	*WNT10B*	*GCAT*	*CCDC122*	*HADHB*
MTOR	*ATP1A2*	*VAPA*	*PTPRM*	*HAUS6*	*EFTUD2*
HRAS	*FARP1*	*UFD1L*	*TRAT1*	*GPR34*	*CCNE2*
KRAS	*MAPRE2*	*TUSC2*	*ATP1B3*	*PTGER2*	*SRSF2*
PRF1	*RAB6A*	*TULP3*	*GUCY2C*	*PCGF6*	*GSTA1*
GZMB	*SH2D2A*	*TTF1*	*CAPN9*	*UHRF1BP1L*	*GNS*
IFNG	*DNA2*	*TSFM*	*NEURL*	*RIBC1*	*FMO5*
HMGCR	*CIT*	*TRHR*	*LOC389493*	*USP46*	*PHKA1*
	PDSS1	*TPBG*	*DISP1*	*MDM2*	*SLC27A2*
	VASH1	*TMEM85*	*GTF2H1*	*PPP1R15B*	*GUCY1A2*
	CBFB	*TMEM30B*	*RAB1A*	*TNPO3*	*PIDD*
	CARHSP1	*TMEM159*	*TIPRL*	*ORC2*	*ALG9*
	UBR7	*TIGD5*	*ZCCHC2*	*NPEPPS*	*UGT2A3*
	TPBG	*THOC7*	*RPN1*	*GRINA*	*CYP2C9*
	CCDC41	*THBS3*	*C9orf41*	*SAMSN1*	*GM2A*
	ANGPTL2	*THAP7*	*MAPRE1*	*VNN1*	*PPP1CA*
	G2E3	*TFEB*	*CEP57L1*	*LARP4*	*GRIN2A*
	RPA2	*TEKT2*	*TMEM161B*	*MIS12*	*PRKACG*
	STIL	*TBPL1*	*CLP1*	*ASZ1*	*LDLRAP1*
	RBM44	*TBC1D23*	*EIF2B3*	*MPHOSPH10*	*RAF1*
	STK39	*TALDO1*	*SSPN*	*PLS3*	*FLT1*
	BMP2K	*SYT7*	*MLF1IP*	*RAD50*	*PRPF38A*
	WDR62	*SYNGR2*	*BTD*	*UBE2Q2*	*GTF2H3*
	SOD1	*SWAP70*	*ST18*	*GNL2*	*PLCD1*
	ICA1	*STX2*	*ACTC1*	*GOLGA7*	*AOC3*

	CA13	*SRPK1*	*MORC2*	*SCN7A*	*NEU1*
	PMCH	*SRMS*	*EEPD1*	*KPTN*	*PMAIP1*
	RPA1	*SPATA5*	*IMP4*	*CEP170*	*ADCY9*
	CLIC4	*SON*	*KCNE3*	*FOLR2*	*SYNJ1*
	CASP7	*SNX2*	*TMEM181*	*CX3CR1*	*DCXR*
	ACTG1	*SLC6A6*	*WDR45L*	*PDE4DIP*	*ABCA1*
	C6orf168	*SLC38A4*	*UMODL1*	*DNM1L*	*BRAF*
	PRICKLE3	*SLC35A2*	*PGM5*	*HELQ*	*GGT1*
	DUSP14	*SLC30A1*	*TRIM66*	*SESTD1*	*PPAP2B*
	POLE	*SLC25A28*	*ZNF18*	*GSPT2*	*GYS2*
	PMVK	*SLC22A12*	*MAB21L3*	*EEF2K*	*ADSSL1*
	FUT4	*SLC20A1*	*GNPDA2*	*FAF2*	*FTMT*
	EXPH5	*SIRT2*	*SEC24D*	*SLC33A1*	*UGT1A5*
	GPD2	*SFTPC*	*SGTA*	*RNF115*	*ACO1*
	LGALS1	*4-Sep*	*MED7*	*PTPLB*	*SDS*
	LSM2	*10-Sep*	*IL1RL1*	*CYSLTR2*	*ENTPD1*
	DAP	*SENP6*	*FTSJD2*	*TERF2IP*	*TREH*
	LCLAT1	*SEMA6C*	*NUDCD1*	*HINFP*	*CDA*
	IL10	*SEC23A*	*LRRC59*	*PTMA*	*GNS*
	MYBL1	*SEC22B*	*AGPS*	*UTP14A*	*ABL1*
	PSMD14	*SAR1A*	*MDH2*	*USP1*	*HADH*
	AMDHD2	*SAA4*	*SBDS*	*NEK4*	*ADH1A*
	EIF4H	*RYK*	*C15orf57*	*TIAL1*	*ITPKB*
	PIF1	*ROBO3*	*LCOR*	*HOOK1*	*NT5C2*
	ACER3	*RNASE3*	*SHCBP1L*	*CASP3*	*PSMD3*
	TPI1	*RGS4*	*TMEM97*	*ATP9B*	*CYP1A1*
	MMD	*RERE*	*CHCHD2*	*NR4A1*	*PRIM2*
	RDBP	*RENBP*	*RGAG4*	*ACACA*	*CRLF2*
	BCAT1	*REG3G*	*PCCB*	*MRFAP1*	*RPS6KA2*
	HIF1A	*RAX*	*C7orf42*	*SBF2*	*MCEE*
	GNB4	*RASA4*	*CKAP2L*	*HNRNPD*	*NRG2*
	FBXO5	*RAB5A*	*RBL1*	*DARS*	*PRPS2*

	KDM2B	*PTPN23*	*RGMA*	*SCNN1G*	*HMGCS1*
	FAM81A	*PSTPIP2*	*SDR42E1*	*PPP1R3B*	*B4GALT1*
	ERBB3	*PSMC1*	*ERP27*	*CBFA2T2*	*DRD4*
	SERPINF1	*PRSS58*	*C21orf91*	*ZC3H15*	*ALDH3A1*
	INTS7	*PRPF8*	*FSCN3*	*CLPX*	*ADRB2*
	RAD51AP1	*PRPF39*	*RBM25*	*TBC1D7*	*PTH2R*
	CENPN	*PRAF2*	*GALNTL5*	*NAV2*	*LYN*
	SRGN	*POU3F3*	*NUDT3*	*HNRPLL*	*MARS*
	TRIP12	*PON1*	*MRAS*	*PRDM5*	*BMPR2*
	GTSF1	*POLR3D*	*SERPINB11*	*SHROOM2*	*CASP3*
	GINS2	*POLR3A*	*SGK1*	*ODF2L*	*CCL26*
	GLRX	*PLAU*	*CDK9*	*IDI1*	*PGK1*
	STAU2	*PIP4K2C*	*MRPS30*	*MRPL32*	*UGT2B10*
	SLC25A20	*PHLDA2*	*PCDHB3*	*VPS33B*	*GGT7*
	SLMO2	*PGAM2*	*BDP1*	*LY96*	*ACSS3*
	FAM111A	*PEMT*	*BDKRB2*	*RFX5*	*GADD45B*
	SHC4	*PCDH7*	*RPAP3*	*SRGAP2*	*PPAP2C*
	DSP	*P2RX6*	*APPBP2*	*GNA13*	*AK7*
	SLC25A10	*OR6A2*	*PLAG1*	*CDC14A*	*ALG12*
	TUBB3	*OPRD1*	*DOPEY1*	*MRGPRF*	*ABL2*
	IL1R2	*OMD*	*NUCB1*	*TMX1*	*EGFR*
	THOC6	*ODZ1*	*SYT12*	*PVT1*	*CCR6*
	DERL2	*NUP62*	*B4GALT7*	*CPEB2*	*PRIM2*
	OSBPL9	*NRCAM*	*CHIC2*	*APAF1*	*WARS*
	ORC6	*NKAIN1*	*BICD2*	*DNAJB2*	*PIP4K2B*
	PRELID2	*NCOA1*	*C20orf94*	*DNAJC3*	*BUB1*
	ANXA7	*NCK2*	*PRKACA*	*SNX16*	*CALM2*
	CHEK1	*NAT6*	*IL12RB1*	*NFYA*	*SETD1A*
	INCENP	*NAB1*	*ST13*	*CENPF*	*CMPK2*
	LITAF	*NAA11*	*TOX3*	*ACER3*	*PLA2G3*
	UBASH3B	*MYT1*	*XPNPEP3*	*TMBIM1*	*JMJD7-PLA2G4B*
	CPD	*KAT7*	*DCTN5*	*TRO*	*CACNA1S*

	RORC	*MYO10*	*GCNT2*	*LAGE3*	*GPAT2*
	UBE2T	*MXI1*	*APIP*	*DTX3*	*ODC1*
	MTCH1	*MTHFR*	*POLR3A*	*KDELC2*	*XCR1*
	HMGN3	*MSH3*	*GTF2F2*	*POMT1*	*POLR2H*
	DEPDC1B	*MRPS7*	*GABARAPL1*	*TBL1X*	*UGT2A1*
	MELK	*MRPS18B*	*XIST*	*ABCA7*	*DCP1A*
	TNFRSF9	*MRPL3*	*DDX20*	*DHX29*	*RFC2*
	HMGB3	*MORC4*	*KIF5B*	*MFSD6*	*ALOX12*
	CYP11A1	*MLLT1*	*CYP4A11*	*POLK*	*ABCD2*
	SPRED1	*MINA*	*CYP2C8*	*CTSD*	*STX19*
	KLHDC2	*MIF4GD*	*RGS13*	*ZHX3*	*PTPLB*
	TSSC1	*MFNG*	*VWC2*	*EIF2AK4*	*PPP3CC*
	H2AFX	*METTL7A*	*RHBDL2*	*USP37*	*TP53AIP1*
	CDC25C	*MEST*	*C19orf28*	*PPAP2A*	*POLD4*
	SLC12A8	*MCM5*	*ATXN1*	*CENPC1*	*DGAT1*
	ZBTB32	*MBD4*	*TAF9*	*SH3BGRL*	*ASNS*
	IL12RB2	*MAST2*	*TOP3B*	*UHMK1*	*SIAH1*
	IFIH1	*MAPKAPK5*	*GNGT1*	*AIFM2*	*PIK3CB*
	DUSP4	*LOC100506612*	*FAM120C*	*SERPINB12*	*HSD17B2*
	C9orf23	*LITAF*	*ACAD8*	*RNF11*	*LOC652346*
	C9orf41	*LGALS9B*	*CCNO*	*ARHGAP5*	*CCL14*
	LRR1	*LEPREL2*	*CERCAM*	*NSMCE2*	*CPS1*
	ABCC4	*LCT*	*PDE4D*	*ADSS*	*CDC5L*
	MAP2K3	*LAMA5*	*TNFAIP6*	*CCDC41*	*STX10*
	RAF1	*LAMA4*	*FAM53B*	*BCAP29*	*SCP2*
	TYMS	*KTN1*	*C17orf108*	*TBC1D5*	*FPGS*
	GCNT1	*KRT6A*	*PAFAH1B1*	*PHACTR4*	*GADD45G*
	GPR25	*KPNA6*	*ALG14*	*SLC30A6*	*LYPLA2*
	CCDC18	*KLF4*	*DACH1*	*LGR4*	*PIGX*
	FHL2	*KLF12*	*MYO3B*	*DEK*	*SEPHS1*
	SMC6	*KCNK3*	*OAZ2*	*FBXW11*	*LDHD*
	PCNA	*KCMF1*	*WNT5A*	*HNRNPA3*	*LIPA*

	ERMN	*ITGAV*	*DNAJB4*	*MMD*	*ADI1*
	C3orf37	*IQGAP2*	*CLIC4*	*ARHGAP12*	*NDUFB6*
	CYB5B	*INMT*	*PIGH*	*SLAMF6*	*ZNRD1*
	PASK	*IL1R1*	*FAM65B*	*RNF25*	*SLC8A1*
	CYTH2	*IL1A*	*ACER2*	*A1CF*	*STMN1*
	PSMD13	*IFIT3*	*CLASP1*	*TPMT*	*CCNE2*
	KIAA1522	*IFIT2*	*U2SURP*	*RAF1*	*MAP2K2*
	ADAP1	*IER3*	*EIF4A1*	*AHRR*	*LTA*
	HMOX1	*IBSP*	*SPG20*		*DCP1B*
	KLC3	*HTR3A*	*GRPEL1*		*RAC2*
	CKAP2L	*HSPA5*	*PPP2R5E*		*ADRA2A*
	EHBP1L1	*HPD*	*SLC1A4*		*PRKACB*
	RTCD1	*HOXB7*	*HNRNPM*		*TCIRG1*
	BRIP1	*GRPEL2*	*BCAS1*		*AARS*
	GSR	*GNPTG*	*C17orf89*		*PLA2G3*
	FAM156A	*GJA4*	*TRIO*		*ADH1A*
	GSTM5	*GFRA1*	*ELN*		*DLAT*
	BCL3	*GABRB1*	*COQ3*		*GOT1*
	SEMA4C	*G0S2*	*KIRREL3*		*GALR2*
	BLM	*FZD9*	*CYP7A1*		*GPX5*
	EPDR1	*FRAT1*	*ALX1*		*UGT2A3*
	ANKRD50	*FOSB*	*DNAJC24*		*COX5A*
	RAPGEF5	*FOLR2*	*BCAP29*		*RPN2*
	TREX1	*FKBP5*	*AMMECR1L*		*CCR2*
	C11orf31	*FKBP10*	*NEU2*		*LPAR3*
	FKBP2	*FGD1*	*CSMD1*		*RPL34*
	FOXM1	*FCER2*	*EGLN3*		*BDH1*
	C11orf51	*FAM110A*	*PSEN1*		*MGAT3*
	SMTN	*EPHB2*	*CEP128*		*PDE6H*
	SNRNP25	*EOMES*	*ASNS*		*GAD2*
	SH3RF1	*ENO1*	*ATF3*		*PSMC6*
	KIF20B	*EIF2B4*	*FLJ37453*		*ACADM*

	STOM	*EFNA5*	*CD80*		*CARS*
	CDKN1A	*E2F5*	*NDUFA12*		*DPYD*
	TOX2	*DVL2*	*VWA3A*		*RPL27A*
	NUP93	*DUT*	*XYLB*		*ARSA*
	EHD4	*DPF3*	*DNAJC12*		*JMJD7-PLA2G4B*
	PTGIR	*DNAJB13*	*C3orf22*		*MDH1*
	POC1A	*DKK3*	*KIAA1161*		*CERK*
	UBL4A	*DEK*	*CLTC*		*TAF9*
	NUCB1	*DEGS1*	*DRGX*		*CD70*
	FMR1	*DDX10*	*ALS2*		*AHCY*
	FIGNL1	*DCAF13*	*NUP43*		*AWAT2*
	ELF4	*CYR61*	*KRT4*		*GFPT1*
	GARS	*CYP2A6*	*QRICH1*		*TGFB1*
	TIMP2	*CTSC*	*C9orf93*		*P4HA1*
	TUFT1	*CSRP1*	*DDX39A*		*LTB4R2*
	SRSF12	*CRX*	*HDHD3*		*LIF*
	KIF18A	*CREBBP*	*SIPA1L1*		*CACNA2D4*
	BEND4	*COX7A1*	*TMED5*		*RPA3*
	AGPAT9	*COL8A1*	*RALYL*		*HAGH*
	C16orf61	*COASY*	*PKD2L2*		*POLR2B*
	NSMAF	*CMA1*	*ANKRD34A*		*S1PR4*
	ARHGAP19	*CLPTM1L*	*CUL3*		*SEC11A*
	GCG	*CLP1*	*TAF1B*		*GRID1*
	EXO1	*CIDEC*	*IL10*		*GPD1L*
	HMMR	*CFI*	*LINC00301*		*AGTR1*
	TUBE1	*CELF1*	*EXOSC8*		*GNPDA2*
	BLMH	*CDV3*	*NAA50*		*FABP7*
	E2F8	*CDKN2D*	*GHSR*		*UGT1A10*
	PRICKLE1	*CD70*	*EIF3B*		*AMDHD2*
	UBXN8	*CCND1*	*EIF2B5*		*LSM3*
	CDC45	*CCL4*	*USP37*		*YWHAH*
	BUB1	*CCKAR*	*YTHDF2*		*CCNB2*

	FRMD4B	*CCDC6*	*OR4E2*		*HGSNAT*
	IQGAP3	*CCDC28B*	*TAL1*		*PPAP2B*
	PYCARD	*CBFA2T3*	*EIF2C3*		*LAPTM4A*
	KIF18B	*CAT*	*SRRM1*		*RAD50*
	RCC1	*CAPZA2*	*LYPLA2*		*CCND2*
	UBR5	*CAMK2D*	*P2RY14*		*ADH5*
	POLH	*CA3*	*MMP3*		*PPCDC*
	C15orf23	*C9orf78*	*CLVS2*		*LAMTOR3*
	CDK2AP1	*C20orf30*	*PAK1IP1*		*GCAT*
	MMP16	*C12orf41*	*ABCC3*		*PSMB11*

Control pathway #2
B4GALT1
LAPTM4B
POLL
TAF2
DHRS9
CAMK2G
ALDH7A1
PLCB3
ALDH9A1
EHHADH
ABCA13
C1GALT1
LCMT2
CCKAR
ALDH9A1
PPP3CA
B3GNT1
UGT2B4
HTR4
RBX1
PNLIPRP2
GALC
CNTF
ATP2B2
FDFT1
DPYS
ABCB8
PSME2
ADORA2B
TRIM37

FGF6
SUOX
HNRNPU
SULT2B1
GALT
QDPR
NAT6
HRH1
DNMT3B
PIK3R1
XAB2
MAP2K7
CLTB
TAB1
DGKQ
RELT
FPGS
MAN2B1
ATP6V0A2
IL15RA
GFPT2
GSTT1
RPA4
IDUA
RNASEH2A
RAC1
BCAT2
CYP26C1
TYMP
BUB3
LOC650621
CDC16

PIK3CD
ATG12
POLR1D
ACOX2
CYP2E1
ACER2
RBKS
RPS9
CCNE1
ALDH2
ATP8
EHHADH
GNG7
EDAR
AP3S2
UGT2B7
COX7A2L
CACNA2D1
IL29
NT5C3
PNP
MGST3
CYP3A5
NT5C1A
CYP1A1
GSTA4
SOAT2
GRB2
ALDH6A1
PRUNE
ATP12A
CDKN2A

IFNGR1
PTH2R
CLTA
GMPR
GUCY2D
LYN
ADCY6
ALDH9A1
ADCY1
CXCL10
MAP2K3
FADS2
GOT1
PGAM4
GSTK1
RPL3
FTCD
UGT1A10
PTAFR
BAAT
SPTLC2
PRKCA
FPR1
UGT2A3
PPAP2A
LPAR2
HTR1A
SYNJ2
ALDH5A1
RYR2
PRIM2
SORD

CHMP4A
GLB1
LTC4S
SFN
RAD50
GK
GDF5
TRPV1
ETNK2
ABCC8
CYSLTR1
MKNK2
CACNA1I
ATP6V1H
RDH11
POLR3D
POLR1A
GGT1
HSD17B12
ALDH2
IDS
AKR1B10
GSTM3
AKT2
DUT
INS
EDC4
OXCT1
ZAK
M6PR
GNG12
UGT1A9

PLD1
TSHR
GLS2
METTL2B
CCNE2
PIGZ
B4GALT4
GNG5
ALDH9A1
ACO2
BCAT1
CES1
UGT1A10
TBXAS1
GRM5
GSTM2
TAF11
VAMP3
IL5RA
ALDH2
PIGG
IFNG
FADS2
IFNA7
HAGH
AMH
TAF4B
ADCY8
GOT1
CHST4
POLR2G
IL4I1

ULK2
PPAP2C
HRH1
TIAM1
CDC42
TREH
UGP2
ITCH
POLR3B
TCIRG1